Journal Name

Dynamic Article Links ►

Cite this: DOI: 10.1039/c0xx00000x

www.rsc.org/xxxxxx

ARTICLE TYPE

Silver Zeolite-Loaded Silicone Elastomers: A Multidisciplinary Approach to Synthesis and Antimicrobial Assessment

Sama Belkhair,[a] Malcolm Kinninmonth,[a] Leanne Fisher,[a] Biliana Gasharova,[b] Christopher M. Liauw,[a] Joanna Verran,[a] Boriana Mihailova[c] and Lubomira Tosheva*[a]

Received (in XXX, XXX) Xth XXXXXXXXX 20XX, Accepted Xth XXXXXXXXX 20XX

DOI: 10.1039/b000000x

A multidisciplinary approach has been applied to the preparation of antibacterial Ag zeolite/silicone elastomer composites aimed at products that satisfy a range of requirements, namely good mechanical properties after zeolite incorporation and strongly antibacterial. Zeolite X was synthesised and used as antibacterial agent after ion-exchange with silver. The high level of silver (14 wt.%) within the zeolite enabled the preparation of antibacterial composites containing a relatively low level of zeolite (2 wt.%). The composites showed strong efficacy against *Escherichia coli* and *Staphylococcus epidermidis*. Organic functionalization of the zeolite with organo-silanes prior blending with the matrix usefully improved composite mechanical properties and reduced color development in Ag zeolite containing silicone elastomers. Organo-silane modification did not substantially affect the antibacterial performance of the materials; the number of viable cells of both Gram-positive and Gram-negative bacteria was reduced to beyond detection limits within 24 hours of incubation. Efficacy of the Ag zeolite containing composites against the yeast *Candida albicans* was found to be substantially less than observed with the two bacteria. This study demonstrates that evaluation of polymer composites needs to be performed via a multidisciplinary approach in order to avoid compromising a particular aspect of the materials' design, characteristics or performance, including the use of reliable testing methods to determine the latter.

Introduction

The use of medical devices has become an essential part of modern day medicine and as a consequence, microbial infections resulting from bacterial adhesion and colonization to biomaterial surfaces is of major concern. The continuously increasing levels of antibiotic resistance have prompted research into adding therapeutic antimicrobials to medical devices with long-term activity to prevent infections.[1] Zeolites are excellent candidates for such applications. They can be exchanged with metal antimicrobials, they are chemically and thermally stable, their pore structure facilitates the slow release of antibacterial metals and also there is a possibility for regeneration upon metal depletion by secondary ion-exchange. Silver is a well-known antibacterial agent with an ability to act on a broad spectrum of organisms.[2] Silver is also the most popular metal of choice for preparation of antibacterial zeolites. The Ag leaching and the antimicrobial activity of Ag-exchanged zeolite A over a 12 month period has been studied by Yan and co-workers.[3] The study demonstrated that Ag zeolite coatings retained their antibacterial activity after 12 months submersion in distilled water and that they were capable of killing *Escherichia coli* (*E. coli*) upon repeated exposures. The killing efficacy of Ag zeolites has been found to depend not only on the silver content but also on the geometry of zeolite pores.[4] Zeolites with a three-dimensional pore system showed superior antibacterial activity compared to one-dimensional zeolites, probably due to the hindered release of Ag in the latter. Further, the antibacterial properties of Ag exchanged into zeolites having the same structure (FAU-type) have been found to differ depending on the Si/Al ratio.[5] Ag-exchanged zeolite Y (Si/Al ratio = 2.83) displayed lower minimum inhibitory concentration against bacteria compared to zeolite X (Si/Al ratio = 1.64), both containing similar Ag loading of 9.7 wt.% and 9.8 wt.%, correspondingly. This result was attributed to the presence of metallic silver in zeolite X. The bactericidal activity of Ag zeolites has also been found to depend on the zeolite physical form, namely powders or zeolite aggregates.[6] Although Ag zeolites of very low Ag loading (0.2 wt.%) have shown high activity against bacteria,[7] higher Ag loadings, 2 wt.% and above, have been typically used.[5,6,8-12]

Silver zeolites have been used as antimicrobial additives for a number of biocompatible polymers at loadings of 1-10 wt.%.[13-20] Amongst these works, only Pehlivan et al. used an organic modifier to improve the compatibility between the polymer and the Ag zeolite, however, the antibacterial properties of the composite films prepared were not reported in their work.[14] Modification of zeolites with silane coupling agents has been extensively studied for the preparation of mixed matrix membranes containing zeolite fillers.[21-23] Despite numerous studies demonstrating the need for organic modification of inorganic fillers in order to avoid interfacial incompatibility (leading often to poor dispersion), Ag zeolites have rarely been modified prior to composite

fabrication.[15-20] Often, only antimicrobial properties have been studied without determining how the mechanical properties of the composites changed upon Ag zeolite loading.[16-19] In addition, in some of the antibacterial tests, it was not evident whether a neutralizer had been used to deactivate silver following incubation of inoculated surfaces.[16-18] We have recently reported that the differences with and without neutralizing the silver can be substantial.[24] In another clinical study, silver zeolite impregnated central vascular catheters have shown a significantly lower colonization rate compared to non-impregnated catheters, however the zeolite type or the silver content were not provided in this paper.[25]

All the above published studies clearly demonstrate that often certain aspects, which can be essential from industrial point of view, are omitted, thereby limiting their usefulness. In this study, a multidisciplinary approach combining three research areas, namely zeolites, polymer science and microbiology, has been applied to prepare and evaluate zeolite containing silicone elastomers. Firstly, a zeolite with a high ion-exchange capacity was synthesized (zeolite X). Silver was ion-exchanged into the zeolite to obtain a high silver loading of ca. 14 wt.% in order to provide sustained Ag release over long periods of time. The Ag zeolite was modified using two organo-silanes and then added to silicone elastomers at 2 wt.%. The antimicrobial effect of the silver zeolite containing polymers was tested against selected organisms. *Staphylococcus epidermidis* (*S. epidermidis*), *Escherichia coli* (*E. coli*) and *Candida albicans* (*C. albicans*) are amongst the organisms, which are recognized to be involved in medical device related infections. Coagulase-negative staphylococci such as *S. epidermidis* are often associated with prosthetic implant infections such as hip and knee replacements,[26] and *E.coli* is one of the main organisms involved in catheter related urinary tract infections.[27] *C. albicans* is an opportunistic organism and a causal agent of infections associated with prosthetic devices in the oral cavity.[28]

Experimental

Synthesis procedures

A batch of NaX zeolite was prepared, and used in all further experiments, from a gel with the molar composition 8NaOH : $0.2Al_2O_3$: $1.0SiO_2$: $200H_2O$.[29] The mixture was homogenized for 1 h, transferred to 500 mL polypropylene bottles and hydrothermally treated at 80 °C for 24 h. The zeolite formed was recovered by filtration, washed with deionized water to obtain a filtrate with neutral pH and dried at 60 °C overnight.

The as-made zeolite NaX was added to 0.05 M silver nitrate solution ($AgNO_3$, Alfa Aesar) at a weight ratio of 1 to 20. The slurry was stirred for 72 h at room temperature. The Ag-exchanged zeolite was filtered and dried at 60 °C overnight. For the preparation of functionalized silver zeolites, 2 g of AgX were mixed with 20 g 10 wt.% solution of 3-(trimethoxysilyl) propylmethacrylate (GE Bayer Silicones) or triethoxy vinylsilane (97%, Aldrich) in cyclohexane and stirred for 30 min at room temperature. The zeolite was then washed several times with cyclohexane by decanting. The modified zeolites were dried at 50 °C for 72 h. The two samples prepared were labelled as M-AgX and V-AgX, correspondingly. All procedures were performed in the dark using foil to cover the glassware.

Composites were prepared from M511 maxillofacial silicone elastomer (SE) (Technovent, UK). The system's components were mixed for 60 s under vacuum using Multivac 4 (Degussa AG, Germany). After a resting time for 15 min, the uncured SE was spread into 13 cm x 13 cm x 0.1 cm metal mold (lined with polyethylene sheet) using a pallet knife. The mold was placed on a vibrating table for 10-15 min to bring the air bubbles to the surface, and the bubbles were burst using a thin wire. The molding was cured at room temperature for 24 h. After curing, the SE was removed from the mold and stored in a plastic bag. A plastic sheet was used in the mold the facilitate the recovery of the cured SE. Zeolite-containing silicone elastomers were prepared similarly after adding 2 wt.% zeolites to the uncured SE mixture. SE containing NaX, AgX, M-AgX and V-AgX were prepared and stored as described.

Characterization methods

The morphology of the zeolites and dispersion quality within the SE/zeolite composites was studied using a JEOL 5600LV Scanning Electron Microscope (SEM). The crystallinity of the zeolites was studied using a PANalytical X'Pert X-ray diffractometer (XRD) employing Cu K_α radiation (40 kV and 30 mA) and a PIXcell detector. Semi-quantitative chemical analysis was performed on uncoated sample pellets by energy-dispersive X-ray spectroscopy (EDS) using a detector from Oxford Instruments. The average of three measurements was used in the determinations. Nitrogen adsorption isotherms were recorded on a Micromeritics ASAP 2020 surface area analyzer at -196 °C. Samples were degassed at 110 °C for 12 h prior to analysis. Specific surface areas were calculated using the BET equation in the 0.05–0.3 range of relative pressures, whereas external surface areas and micropore volumes were determined by the t-plot method. Powder samples diluted in KBr were examined by diffuse reflectance Fourier transformed infrared (DRIFT) spectroscopy using a Thermo Nicolet Nexus FT-IR spectrometer fitted with a Spectra-Tech DRIFTS cell (Thermo Fisher Scientific, Waltham USA). DRIFT spectra were measured be-tween 400 and 4000 cm^{-1} with an instrumental spectral resolution of 4 cm^{-1} using 160 scans. Raman-scattering experiments were performed on NaX and AgX zeolite powders with a Horiba Jobin-Yvon T64000 triple-grating spectrometer equipped with a LN_2-cooled Symphony CCD detector and an Olympus BH41 microscope with a 50x long-working distance objective. Spectra in the range 15 - 4000 cm^{-1} were collected in backscattering geometry using the 514.5 nm line of an Ar^+-ion laser (Coherent Innova 90C FreD). The laser power on the sample surface was 5.9 mW, while the diameter of the laser spot on the sample surface was approximately 2 μm. No polarization, orientation, or spatial dependence of the Raman spectra was detected, indicating that the average linear crystallite size is much smaller than linear size of the probed sample volume. The achieved spectral resolution was 1.9 cm^{-1}, while the precision in the peak positions was 0.35 cm^{-1}. The measured spectra were baseline corrected for the continuum photoluminescence background, temperature-reduced to account for the Bose-Einstein occupation factor and then the spectral range 15-650 cm^{-1} was fitted with Lorentz functions to accurately determine the peak positions, full widths at half maximum (FWHMs) and intensities.

To check whether Ag enters the zeolite structure in mono- or divalent ionic form, Fourier transform infrared (FTIR) spectroscopic experiments in the far-IR range (50-550 cm^{-1}) were conducted on NaX and AgX powders as well as on reference mechanical mixtures of NaX with 10 wt.% commercial Ag(I) (99.99%, Alfa Aesar) and Ag(II) (98%, Alfa Aesar) oxides. FTIR spectra were measured in transmission with a Bruker IFS66 v/S equipped with a Globar white source, a DTGS detector, and a 6-μm Si/Mylar beamsplitter. In order to avoid artificial absorption bands from rotation transitions of atmospheric molecules, in particular from H_2O molecules, the far-IR spectra were measured in the sample compartment under a vacuum of 3 mbar. Samples have been prepared as ethanol suspensions, placed onto Si windows (Korth, 400 μm thick, wedged) and the ethanol evaporated off. A background spectrum was collected from a clean Si window. The mirror scanning velocity was 5 kHz and the instrumental spectral resolution was 4 cm^{-1}. Spectra were averaged over 32 scans. An attempt was made using synchrotron IR radiation (IR2 beamline at ANKA/KIT) to collect far-IR spectra from individual zeolite particles NaX, AgX, M-AgX, and V-AgX before and after their incorporation into elastomers. An IR microscope, sealed in a home-made compartment and purged with N_2 gas was used for the analysis. Although the humidity was reduced to ~ 3%, the spectral range below 300 cm^{-1} was still confounded by the H_2O rotation bands, which prevented definitive interpretation.

Hexane (Fisher) swelling measurements on the composite samples were carried out at ambient temperature. Sample dimensions were 1 x 2 x 0.1 cm and the immersion was for 24 h. After immersion, excess hexane was removed from samples before weighing using filter paper. Degree of swelling was calculated using the following equation:

$$\text{Swelling degree}(\%) = \frac{\text{weight before} - \text{weight after}}{\text{weight before}} \text{x} 100$$

For tensile testing, dumbbell specimens with a width of 3.6 mm were cut from the approximately 1 mm thick SE sheets. A universal testing machine, Tensometer 2000 (Alpha Technologies), was used and the tensile tests were carried out at a crosshead speed of 500 mm min^{-1}. The dumbbell specimens were placed within the tensile grip, with a separation of 20 mm between them. Prior to testing, the thickness of each specimen was measured using a digital caliper at the center and at the ends. The tensometer measured extension of samples and a 100 N load cell measured the applied force. Five samples per compound were tested.

Antimicrobial tests

A single colony of *E. coli* (ATCC 8739) or *S. epidermidis* (NTCC 11046) from a freshly cultured nutrient agar (Oxoid, UK) plate was removed using a sterile loop and inoculated in 100 mL nutrient broth (Oxoid, UK). The broth was incubated for 18-24 hours in a 37 °C rotary shaker incubator set at 150 rpm. The liquid culture was centrifuged at 3000 rpm for 10 min to form a pellet. The supernatant was discarded and the pellet was re-suspended in sterile ringers solution (Oxoid, UK). An optical density of 1.0 at 540 nm wavelength was obtained, and a 1:10 dilution was performed in ringers solution. This suspension was used to inoculate the surfaces. The dimension of the SE test pieces was 20 mm x 10 mm. Test pieces were sterilized by autoclaving at 121 °C for 15 min prior to use and each sample placed in a separate sterile petri dish. The antimicrobial activity of test specimens was carried out using ISO 22196 standard (Measurement of antibacterial activity on plastics and other non-porous surfaces) as guidance. 50 μL of the standardized bacterial suspension (4 x 10^6 colony forming units (CFU) mL^{-1} for *E. coli* and 2 x 10^5 CFU mL^{-1} for *S. epidermidis*, respectively) was pipetted onto the sample surface. A 20 mm x 10 mm polyethylene film was placed on top and gently pressed down to ensure the bacteria spread evenly on the surface; care was taken to ensure the bacteria did not leak beyond the edges of the film. Immediately after inoculation, surfaces were placed individually into 10 mL neutralizing agent (14.6% sodium thiosulphate and 10% sodium thioglycollate in 100 mL distilled water; 5 mL was filter sterilized into 495 mL sterile distilled water)[30] and vortexed for 30 s to detach bacteria. The neutralizing agent acts to neutralize the bactericidal effect of the silver at the selected time points. We have demonstrated previously that the silver continues to exert its killing effect on the bacteria after the test time in the absence of a neutralizing agent.[24] Bacteria were enumerated by serial dilution (1:10) and plating followed by CFU determination. 100 μL were spread onto nutrient agar plate and plates were incubated overnight at 37 °C. Colony counts were per-formed and CFU mL^{-1} were calculated using the equation:

$$\text{CFU mL}^{-1} = \frac{\text{CFU x Dilution factor}}{\text{volume plated in mL}} \text{x} 100$$

The remaining surfaces in Petri dishes were incubated at 37 °C and tested as above at 5 and 24 hours. The value of viable counts was determined from an average of the counts on three inoculated surfaces.

The same procedure was applied for *C. albicans* (NCYC 1363) but the overnight growth was performed in sabouraud dextrose liquid medium (Oxoid, UK). 50 μL of the standardized *Candida* suspension (2 x 10^4 CFU mL^{-1}) was inoculated onto the test pieces. Serial dilutions (1:10) were made as above and 100 μL were plated out onto sabouraud dextrose agar. The surfaces were incubated at 37 °C and tested at 0, 24 and 48 hours.

A 2 tailed homoscedastic Student's t-test was per-formed using Microsoft Excel 2013 to compare antimicrobial test data sets. If the *p*-value was less than 0.05, then results were statistically significant.

Results and discussion

Zeolite characteristics

The zeolite NaX prepared had a Si/Al ratio of 1.4. SEM analysis indicated that the sample was highly crystalline and free from impurities of other phases (Fig. 1a,c). The crystal sizes ranged between 400 nm and 3.5 μm. The introduction of Ag and the functionalization with organic silanes did not influence the morphology or the crystal size distribution of the zeolite samples (Fig. 1b,d). EDS analysis showed that 86% of the Na in NaX (15.9 wt.%) was ion-exchanged with Ag in AgX (Table 1). The Si/Al ratio of 1.4 for NaX slightly increased as a result of the modification procedures to 1.5 for AgX and M-AgX and 1.7 for V-AgX, respectively, indicating that there may be a certain degree of Al leakage. However, EDS analysis does not allow quantification of

Table 1. Ag content, BET surface area (S_{BET}), micropore volume (V_{μ}) and external surface area (S_{EXT}) of zeolite and modified zeolite samples

Sample	Ag, wt.%	S_{BET}, m^2g^{-1}	V_{μ}, cm^3g^{-1}	S_{EXT}, m^2g^{-1}
NaX	-	570.7	0.26	43.1
AgX	14.1	510.6	0.23	40.6
V-AgX	9.6	449.6	0.20	42.5
M-AgX	8.8	351.2	0.16	18.3

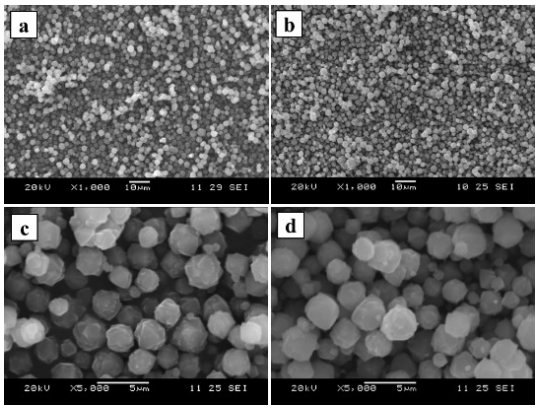

Fig. 1 SEM images at two different magnifications of (a,c) zeolite NaX and (b,d) typical SEM images of organically modified AgX crystals.

the degree of Al leakage. The Ag content of zeolite samples decreased as a result of silane treatment (Table 1), and a C content of ca. 6 wt.% was detected in both M-AgX and V-AgX samples.

The phase purity was further confirmed by XRD analysis (Fig. 2). All observed Bragg peaks in the XRD patterns of all four samples could be indexed to the FAU-type zeolite structure.[31] Ag ion-exchange resulted in negligible change in the Bragg peak positions and widths, indicating high degree of crystallinity for all four samples. The substitution of Ag for Na only changed the relative intensity of some diffraction peaks, which was most pronounced for the (220), (311) and (331) faujasite peaks. In the XRD pattern of NaX, the intensity decreased in the order I(220) > I(331) > I(311), whereas in the XRD pattern of all AgX zeolites, the order was I(311) > I(220) > I(331). The relative intensity variations are related to the change in the charge-balancing cations from Na to Ag.[5]

The gas adsorption data are shown in Fig. S1 (ESI), and Table 1. Nitrogen adsorption isotherms were all type I isotherms typical of microporous materials suggesting that the Ag ion-exchange and organic modification did not change the nature of the samples' pore structures. However, there was a progressive decrease in the micropore volume in the order NaX > AgX > V-AgX > M-AgX. The external surface area of all zeolites was similar except for the M-AgX. Considering the XRD results, the decrease of the micropore volume is most likely due to the larger ionic radius of Ag^+ compared to Na^+ as well as inaccessibility of the nitrogen adsorbate gas to the pore structure of silane-modified samples and not due to loss of crystallinity.

The organic modification was further studied by DRIFT analysis (ESI Fig. S2). First, all zeolite bands in the range 460 – 1100 cm^{-1} remained unchanged confirming preservation of the zeolite structure in the modified samples. The organic modification resulted in additional C-H bands in the range 1200 – 1500 cm^{-1}, which were more evident in the spectrum of M-AgX, and also bands in the range 2800 – 3000 cm^{-1} for M-AgX.[22,32] In addition, a shoulder at 1700 cm^{-1} was present in spectrum of M-AgX,

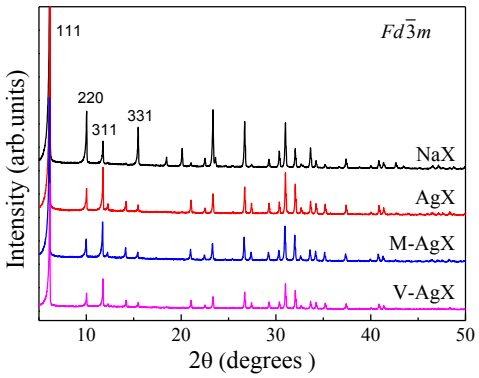

Fig. 2 XRD patterns of NaX and Ag-containing zeolites. Miller indices are given in $Fd\bar{3}m$.

associated with the carbonyl C=O group of the M modifier.[33] The organic functionalization was further proved by the ability to obtain dispersions of V-AgX and M-AgX in chloroform and their aggregation in distilled water (ESI Fig. S3).

Figure 3a shows the Raman spectra of NaX, AgX, V-AgX, and M-AgX samples. The Raman spectra of the silane-modified samples V-AgX and M-AgX resembled the Raman spectrum of AgX, i.e. the influence of the organic modifier on the skeleton vibrations was negligible. All three Ag-exchanged samples showed the same spectral differences in the range of framework vibrations as compared to NaX: (i) slight shift of the main Raman peak near 510 cm^{-1} towards lower energies accompanied with a slight broadening (see Fig.3b) and (ii) additional weak peaks near 570 and 600 cm^{-1}.

The strongest peak in the Raman spectrum of zeolite X is generated by the double 6-membered rings (D6Rs) typical of FAU framework topology.[34] Previous single-crystal XRD analysis of Ag-exchanged FAU has revealed that a large part of the incorporated Ag^+ ions are accommodated in the D6Rs.[35] On the other hand, a lower-energy shift and broadening of the peak near 510 cm^{-1} along with appearance of a peak near 570 cm^{-1} due to the existence of single 4-membered rings (S4R) has been observed in amorphous FAU.[34,36] Raman scattering in the vicinity of 600 cm^{-1} is typical of small 3-membered rings in amorphous framework silicates.[37] Therefore, the Raman data presented here indicate that the incorporation of Ag in part induces local structural defects, but otherwise the overall zeolite framework topology is preserved. The Raman scattering in the range 3200-3600 cm^{-1}, originating from O-H bond stretching is suppressed in the spectrum of AgX. Thermogravimetric analysis showed a negligible reduction in the water content of AgX compared to NaX (ESI Fig. 4S) indicating that this region of the Raman spectra was very sensitive to variations in the samples' water content. The level of photoluminescence background above 3000 cm^{-1} was unfortunately too high for M-AgX and V-AgX to draw any conclusions about H_2O in the pores of these two samples.

The comparison of far-IR spectra of AgX with the spectra of reference mechanical mixtures of zeolite NaX and monovalent and divalent silver oxides (Fig. 4) indicate that indeed Ag enters the zeolite structure in a monovalent ionic form, in accordance with the results from single-crystal XRD analysis[34] and EXAFS analysis.[38]

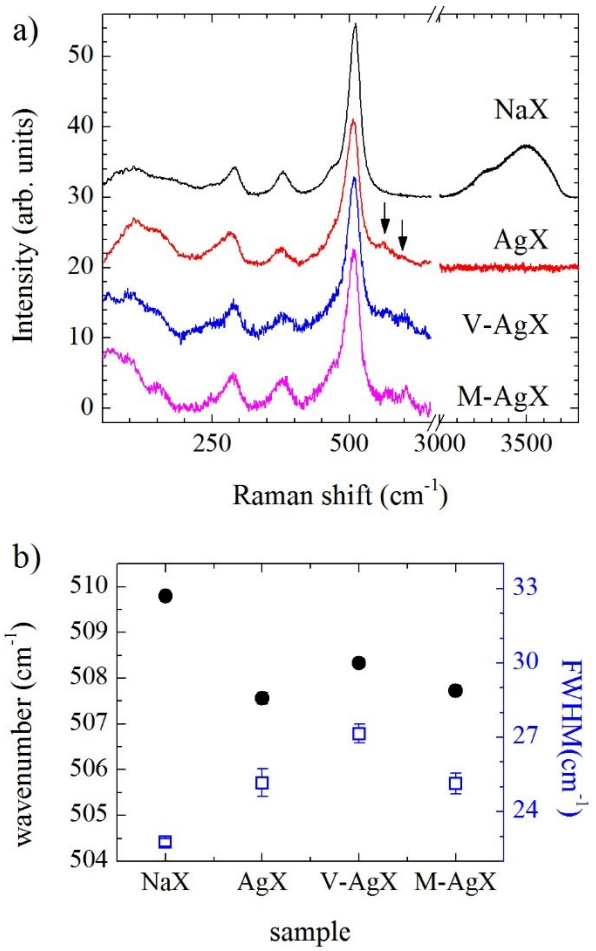

Fig. 3 a) Raman spectra of NaX, AgX, V-AgX and M-AgX; spectra are vertically offset for clarity. The arrows mark the additional peaks observed in all Ag-exchanged samples. b) Position and FWHM of the strong peak near 510 cm^{-1} as determined by fitting the spectra.

Silicone elastomers

Zeolite and modified zeolite samples were added to silicone elastomers at 2 wt.% loading. Digital images of the obtained polymers are shown in Fig. 5. The elastomers containing NaX and AgX without organic functionali-zation contained aggregated particles, whereas the polymers prepared with the addition of functionalized AgX (M-AgX and V-AgX) appeared rather homogeneous. The color of all elastomers containing Ag zeolite particles was darker compared to the neat SE. However, AgX/SE and M-AgX/SE appeared yellow-brownish, whereas V-AgX/SE seemed to be considerably less colored, approaching the overall appearance of NaX/SE. Since the amount of Ag in M-AgX is slightly larger than that in V-AgX (Table 1), the concentration of Ag cannot be the sole reason for the color differences observed between M-AgX/SE and V-AgX/SE. Brownish discoloration of polymers upon addition of Ag has been observed before and attributed to the reduction of silver within the polymer.[19] A combined computational and experimental study of the electronic structure of d^{10}-ion-exchanged zeolites has demonstrated that the color of evacuated (H_2O-free) silver containing sodium zeolite X changes to yellowish/reddish due to electronic transition between Ag^+ and the lone pair of adjacent O from the four-membered rings

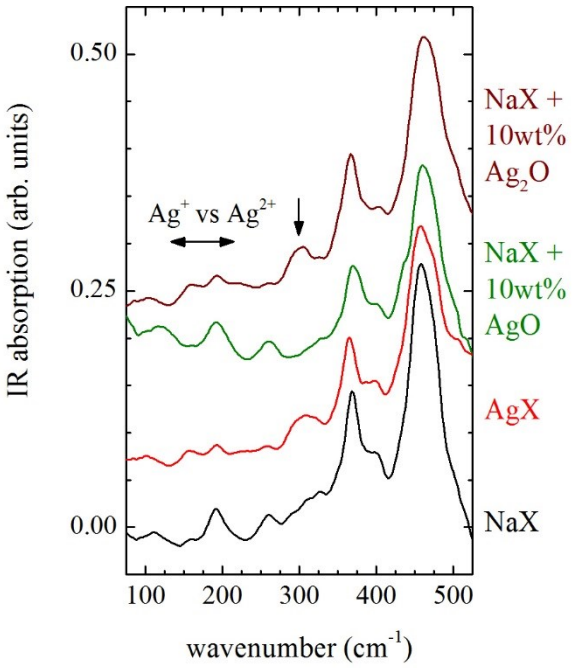

Fig. 4 Far-IR absorption spectra of zeolite X (NaX) and Ag-exchanged zeolite X (AgX) as well as of reference mechanical mixtures of zeolite X with 10 wt.% Ag(I) oxide (NaX + 10 wt.% Ag_2O) and Ag(II) oxide (NaX + 10 wt.% AgO). The arrows mark the spectral bands that can discriminate monovalent and divalent Ag^{n+}. Spectra are vertically offset for clarity.

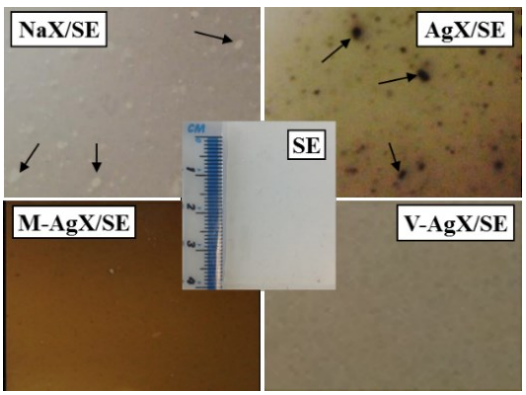

Fig. 5 Digital images of silicone elastomers containing NaX, AgX, M-AgX and V-AgX zeolites. The middle image shows the neat SE. The arrows point to zeolite aggregates present in samples NaX/SE and AgX/SE.

in the absence of H_2O.[39] The reduction of H_2O in the zeolite pores during the preparation of the silicone elastomers maybe the reason for the brownish colorization observed in AgX/SE. In the case of M-AgX/SE and V-AgX/SE, organic functionalization may have partially prevented the water from leaving the zeolite channels during preparation thus reducing the degree of colorization, which reduction was more pronounced for the V-AgX/SE sample.

SEM images of cryo-fractured SE/zeolite composite fracture surfaces (Fig. 6) supported visual observation of poor zeolite dispersion (Fig. 5). Zeolite aggregates and poor filler-matrix adhesion are apparent in NaX/SE and AgX/SE (Fig. 6a). In contrast, composites based on the organo-silane treated zeolite showed good filler dispersion and good filler – matrix adhesion (Fig. 6b).

Table 2 Swelling degree and mechanical properties of the silicone elastomers prepared

Sample	Swelling degree, %	Tensile strength, MPa	Break %
SE	1.77	5.98±0.56	661.6±65.00
NaX/SE	3.74	3.01±0.78	557.5±91.55
AgX/SE	3.09	4.50±0.26	523.1±42.86
V-AgX/SE	1.79	5.63±0.51	694.4±42.45
M-AgX/SE	1.88	5.89±0.31	649.5±21.00

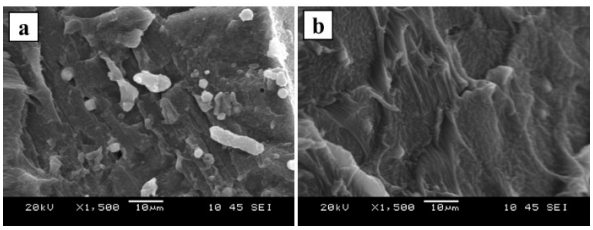

Fig. 6 Typical SEM images of cryo-fractured surfaces of SE/zeolite composite containing: (a) unmodified zeolite (NaX or AgX) and (b) organo-silane modified Ag zeolite (M-AgX and V-AgX gave similar images).

The hexane swelling characteristics and the mechanical properties of the composites and unfilled matrix are given in Table 2. The degree of swelling was lower when organo-silane modified NaX or AgX were added to SE; this is entirely consistent with increased filler – matrix interaction. The latter is confirmed by the improved mechanical properties arising from organo-silane modification, which is also supported by the fracture analysis (Fig. 6). These results indicated that the coupling agents improved the compatibility between the zeolite and the polymer and resulted in high quality SE/zeolite composites.

Antimicrobial activity

The antibacterial activity of Ag-containing silicone elastomers was tested against Gram-negative *E. coli* (Fig. 7) and Gram-positive *S. epidermidis* (Fig. 8) after 0, 5 and 24 h of incubation. The SE and NaX/SE samples did not show any antibacterial activity in all tests. For the AgX/SE samples, *E. coli* counts were reduced from > 10^5 CFU mL^{-1} to below the limit of viable cell detection of <10 CFU mL^{-1} within 24 hours, and *S. epidermidis* was reduced from > 10^4 CFU mL^{-1} to < 10 CFU mL^{-1} within 24 hours. There were some variations in the killing efficacy of *S. epidermidis* after 5 h for the different Ag containing samples, but these were not significant (p > 0.05). The bactericidal mechanism of silver ions against *E. coli* and *S. aureus* has been studied by Feng et al.[40] The authors attributed the inhibitory effect of Ag^+ to loss of replication abilities of the DNA molecules and inactivation of the bacterial proteins as a result of a reaction between the silver ions and the protein thiol groups. In addition, similar morphological changes were observed in the two types of bacteria but the Gram-positive *S. aureus* demonstrated a stronger defense system against Ag^+. These results may explain the greater reduction in the number of viable *E. coli* cells after 5 h of incubation compared to that of *S. epidermidis* on SE containing functionalized Ag-zeolites. This was not observed for SE/Ag zeolite samples, probably because of local fluctuations in Ag concentration in test pieces as a result of the presence of aggregates in this sample (Fig. 5).

The antimicrobial activity of the samples against the yeast *C. albicans* was determined after 0, 24 and 48 h of incubation (Fig.

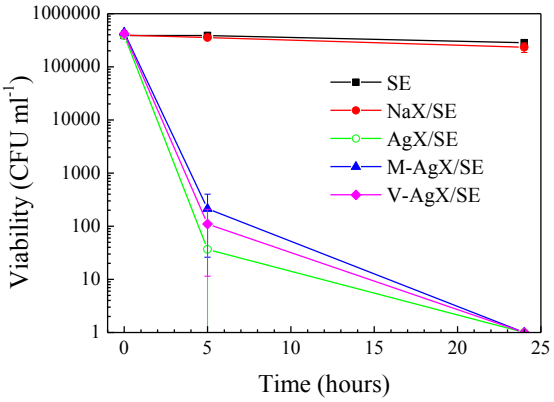

Fig. 7 Viable bacterial cell counts of *E. coli* in the presence of SE and SE containing zeolites.

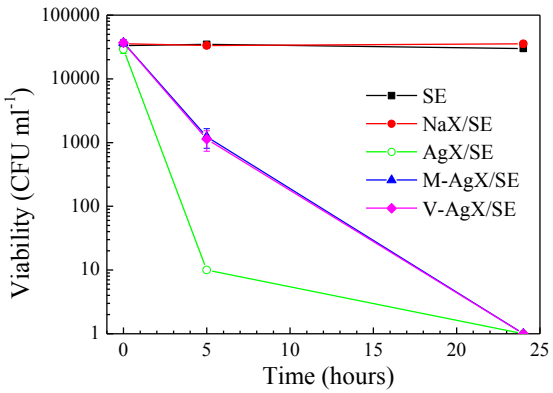

Fig. 8 Viable bacterial cell counts of *S. epidermidis* in the presence of SE and SE containing zeolites.

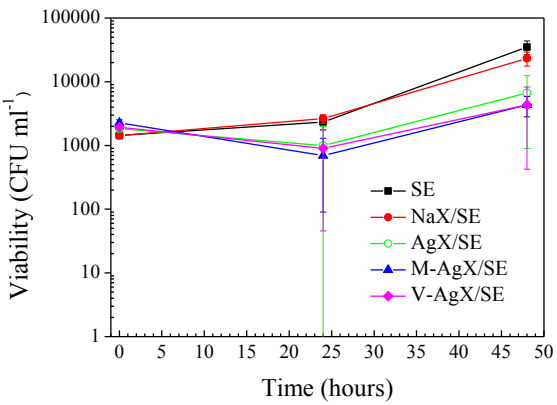

Fig. 9 Viable bacterial cell counts of *C. albicans* in the presence of SE and SE containing zeolites.

9). *C. albicans* was found to be less sensitive to the action of Ag containing samples compared to bacteria. A small decline in the number of viable cells was observed over the first 24 h for all test samples, although this was only significant when comparing V-AgX/SE at 0 h to 24 h (p = 0.014). At the 48 h sampling time, an increase of *C. albicans* on the test surfaces was apparent, although

again only significant when comparing V-AgX/SE at 24 h to 48 h. The reason for this slight increase may be because *C. albicans* reproduces by budding followed by release of daughter cells, which could have led to the higher colony count. The results in Fig. 9 suggest that the Ag^+ concentration released from the polymers is not high enough to kill yeast. Eukaryotic yeast cells are larger and more complex than prokaryotic bacterial cells, and are less sensitive to many antimicrobial agents. Ferreira et al. found that Ag-containing FAU-type zeolites displayed higher minimum inhibitory concentrations for yeast compared to bacteria.[5] It is therefore likely that an increase in the Ag-zeolite loading in the SE could also lead to greater efficacy against *C. albicans*. However, this was not an objective of the present study.

An attempt was made to determine the concentrations of released Ag from the different surfaces prepared after immersion in distilled water (ESI). Silver concentrations were determined to be around 0.005 ppm for all surfaces and no trends could be established for the influence of the samples' type or the exposure time on the concentrations of released Ag. Greulich et al. have reported that silver ions can be toxic not only to bacterial but also to human cells in the concentration range 0.5 to 5 ppm of silver.[41] The determination of the toxicity of the materials reported in this work towards mammalian cells is of paramount importance for a biomedical application and will be addressed in a future study.

Conclusions

A multidisciplinary approach was applied to the development of antibacterial silicone elastomers (SE)/zeolite composites. Silver-zeolite X was prepared and incorporated into silicone elastomers after organo-silane modification. Raman spectroscopy revealed that Ag ion-exchange of the zeolites introduced local structural defects, however the overall zeolite structure was preserved. Far-IR analysis indicated that Ag was present in monovalent form. Organo-silane modification of the zeolite was found to be essential for retention of composite mechanical properties, relative to the unfilled matrix. The latter, together with reduced swelling in hexane and SEM evidence, indicated that organo-silane modification lead to improved filler-matrix interaction. Reduction of ionic Ag to metallic Ag led to discoloration of the SE/Ag zeolite composites. Organo-silane modification led to a decrease in the extent of discoloration; interestingly this effect was strongest with the vinyl silane. The antibacterial tests revealed 4 to 3-log reductions in the viability of *E. coli* and *S. epidermidis* (after 24 h of incubation), respectively, on contact with SE/Ag zeolite composites. *C. albicans* was less sensitive to the test materials than the bacteria tested. A higher concentration of agent might prove more effective against this microorganism. The composites prepared could potentially be used for medical devices featuring long-term antibacterial activity to prevent infections. The present work and previous research clearly demonstrate that a multidisciplinary approach is required for preparation and evaluation of antimicrobial polymers containing inorganic fillers in order to avoid compromising key aspects, e.g., zeolite characteristics, polymers mechanical properties and physical appearance or use of reliable antimicrobial tests.

Acknowledgements

We acknowledge the Synchrotron Light Source ANKA for provision of instruments at their beamlines and we would like to thank Michael Süpfle for assistance in using beamline IR2. The research leading to these results has received fund-ing from the European Community's Seventh Framework Programme (FP7/2007-2013) under grant agreement No. 312284.

Notes and references

[a] *Faculty of Science and Engineering, Manchester Metropolitan University, Chester St., Manchester, M1 5GD, UK. Fax:+44 (0)161 2476840; Tel:+44 (0)161 2471426; E-mail: l.tosheva@mmu.ac.uk*
[b] *Institute for Photon Science and Synchrotron Radiation, Karlsruhe Institute of Technology, P.O. Box 3640, Karlsruhe 76021, Germany*
[c] *Mineralogisch-Petrographisches Institut, Universität Hamburg, Grindelallee 48, D-20146 Hamburg, Germany*

† Electronic Supplementary Information (ESI) available: Nitrogen adsorption isotherms and DRIFT spectra of NaX, AgX and silane-modified AgX samples. See DOI: 10.1039/b000000x/

1 A. Muñoz-Bonilla and M. Fernández-García, *Prog. Polym. Sci.*, 2012, **37**, 281-339.
2 S Chernousova and M. Epple, *Angew. Chem. Int. Ed.*, 2013, **52**, 1636-1653.
3 R. S. Bedi, R. Cai, C. O'Neill, D. E. Beving, S. Foster, S. Guthrie, W. Chen and Y. Yan, *Microporous Mesoporous Mater.*, 2012, **151**, 352-357.
4 P. Saint-Cricq, Y. Kamimura, K. Itabashi, A. Sugawara-Narutaki, A. Shimojima and T. Okubo, *Eur. J. Inorg. Chem.*, 2012, 3398-3402.
5 L. Ferreira, A. M. Fonseca, G. Botelho, C. Almeida-Aguiar and I. C. Neves, *Microporous Mesoporous Mater.*, 2012, **160**, 126-132.
6 P. Lalueza, M. Monzón, M. Arruebo and J. Santamaría, *Mater. Res. Bull.*, 2011, **46**, 2070-2076.
7 P. Lalueza, M. Monzón, M. Arruebo and J. Santamaría, *Chem. Commun.*, 2011, **47**, 680-682.
8 B. Kwakye-Awuah, C. Williams, M. A. Kenward and I. Radecka, *J. Appl. Microbiol.*, 2008, **104**, 1516-1524.
9 R. Guerra, E. Lima, M. Viniegra, A. Guzmán and V. Lara, *Microporous Mesoporous Mater.*, 2012, **147**, 267-273.
10 C. Caroline, B. J. Carlos, B. M. L. Zapata and Z. J. Manuel, *Microporous Mesoporous Mater.*, 2014, **188**, 118-125.
11 Y. Zhou, Y. Deng, P. He, F. Dong, Y. Xia and Y. He, *RSC Adv.*, 2014, **4**, 5283-5288.
12 L. Tosheva, A. Brockbank, B. Mihailova, J. Sutula, J. Ludwig, H. Potgieter and J. Verran, *J. Mater. Chem.*, 2012, **22**, 16897-16905.
13 D. R. Monteiro, L. F. Gorup, A. S. Takamiya, A. C. Ruvollo-Filho, E. R. de Camargo and D. B. Barbosa, *Int. J. Antimicrob. Agents*, 2009, **34**, 103-110.
14 H. Pehlivan, D. Balköse, S. Ülkü and F. Tihminlioğlu, *Compos. Sci. Technol.*, 2005, **65**, 2049-2058.
15 K. Kamişoğlu, E. A. Aksoy, B. Akata, N. Hasirci and N. Baç, *J. Appl. Polym. Sci*, 2008, **110**, 2854-2861.
16 P. Kaali, E. Strömberg, R. E. Aune and G. Czél, *Polym. Degrad. Stabil.*, 2010, **95**, 1456-1465.
17 A. Fernández, E. Soriano, P. Hernández-Muñoz and R. Gavara, *J. Food Sci*, 2010, **75**, E186-E193.
18 D. Zampino, T. Ferreri, C. Puglisi, M. Mancuso, R. Zaccone, R. Scaffaro and D. Bennardo, *J. Mater. Sci.*, 2011, **46**, 6734-6743.
19 D. L. Boschetto, L. Lerin, R. Cansian, S. B. C. Pergher and M. Di Luccio, *Chem. Eng. J.*, 2012, **204-206**, 210-216.
20 K. Tapmin and N. Sombatsompop, *J. Vinyl Addit. Technol.*, 2013, **12**, 113-122.
21 D. Metin, F. Tihminlioğlu, D. Balköse and S. Ülku, *Compos. Part A*, 2004, **35**, 23-32.
22 P. Wei, X. Qu, H. Dong, L. Zhang, H. Chen and C. Gao, *J. Appl. Polym. Sci.*, 2013, **128**, 3390-3397.
23 D. Bastani, N. Esmaeili and M. Asadollahi, *J. Ind. Eng. Chem.*, 2013, **19**, 375-393.
24 B. Dong, S. Belkhair, M. Zaarour, L. Fisher, J. Verran, L. Tosheva, R. Retoux, J.-P. Gilson and S. Mintova, *Nanoscale* 2014, **6**, 10859-10864.

25 M. D. Khare, S. S. Bukhari, A. Swann, P. Spiers, I. McLaren and J. Myers, *J. Infection*, 2007, **54**, 146-150.
26 R. D. Inman, K. V. Gallegos, B. D. Brause, P. B. Redecha and C. L. Christian, *Am. J. Med.*, 1984, **77**, 47-53.
27 T. M. Hamill, B. F. Gilmore, D. S. Jones and S. P. Gorman, *Expert Rev. Med. Devices*, 2007, **4**, 215-225.
28 M. J. McCullough, B. C. Ross and P. C. Reade, *Int. J. Oral Maxillofac. Surg.*, 1996, **25**, 136-144.
29 V. P. Valtchev and K. N. Bozhilov, *J. Phys. Chem. B*, 2004, **108**, 15587-15598.
30 R. C. Tilton and B. Rosenberg, *Appl. Environ. Microbiol.*, 1978, **35**, 1116-1120.
31 W. H. Baur, *Am. Mineral.*, 1964, **49**, 697-704.
32 S. Yi, Y. Su and Y. Wan, *J. Membr. Sci.*, 2010, **360**, 341-351.
33 Q. Yao and Y. Zhou, *J. Inorg.Organomet. Polym.*, 2009, **19**, 215-222.
34 S. Inagaki, K. Thomas, V. Ruaux, G. Clet, T. Wakihara, S. Shinoda, Y. Kubota and Valtchev, *ASC Catal.*, 2014, **4**, 2333-2341.
35 S. Y. Kim and Y. Kim, *J. Phys Chem. B*, 2003, **107**, 6938-6945.
36 J. Catafesta, F. Alabarse, C. Levelut, A. Isambert, P. Hébert, S. Kohara, D. Maurin, J.-L. Bantignies, O. Cambon, G. Creff, P. Roy, J.-B. Brubach, T. Hammouda, D. Andrault and J. Haines, *Phys. Chem. Chem. Phys.*, 2014, **16**, 12202-12208.
37 L. Tosheva, B. Mihailova, V. Valtchev and J. Sterte, *Microporous Mesoporous Mater.*, 2000, **39**, 91-101.
38 S. G. Aspromonte, M. D. Mizrahi, F. A. Schneeberger, J. M. R. López and A. V. Boix, *J. Phys. Chem. C*, 2013, **117**, 25433-25442.
39 G. Calzaferri, C. Leiggener, S. Glaus, D. Schürch and K. Kuge, *Chem. Soc. Rev.*, 2003, **32**, 29-37.
40 Q. L. Feng, J. Wu, C. Q. Chen, F. Z. Cui, T. N. Kim and J. O. Kim, *J. Biomed. Mater. Res.*, 2000, **52**, 662-668.
41. C. Greulich, D. Braun, A. Peetsch, J. Diendorf, B. Siebers, M. Epple and M. Köller, *RSC Adv.*, 2012, **2**, 6981-6987.

